Petroleum Science 23 (2026) 2793–2807

Contents lists available at ScienceDirect

Petroleum Science

journal homepage: www.keaipublishing.com/en/journals/petroleum-science

Original Paper

Microscopic experiments and simulations of CO_2 huff-n-puff displacement mechanism considering heterogeneity and fractures

Nan Chen [a,b,c,d], Chuan-Jin Yao [a,c,d,*], Bai-Shuo Liu [a,c,d], Jia Zhao [a,c,d], Cui-Fang Li [a,c,d]

[a] State Key Laboratory of Deep Oil and Gas, China University of Petroleum (East China), Qingdao, 266580, Shandong, China
[b] School of Energy and Power Engineering, Xi'an Jiaotong University, Xi'an, 710049, Shaanxi, China
[c] School of Petroleum Engineering, China University of Petroleum (East China), Qingdao, 266580, Shandong, China
[d] Key Laboratory of Unconventional Oil & Gas Development (China University of Petroleum (East China)), Ministry of Education, Qingdao, 266580, Shandong, China

ARTICLE INFO

Article history:
Received 9 November 2024
Received in revised form
6 March 2026
Accepted 8 March 2026
Available online 14 March 2026

Edited by Yan-Hua Sun

Keywords:
Carbon dioxide enhanced oil recovery (CO_2 EOR)
Huff-n-puff
Heterogeneity
Fracture
Carbon capture, utilization, and storage (CCUS)

ABSTRACT

Heterogeneity and fractures significantly influence oil and gas migration. However, current research remains insufficient in clearly visualizing CO_2 displacement mechanisms under such reservoir conditions. This study combines microscopic visualization experiments and numerical simulations to investigate three-phase flow characteristics during CO_2 huff-n-puff, CO_2 displacement, and water huff-n-puff in heterogeneous fractured reservoirs. The research elucidates the formation mechanism of residual oil and the characteristic of CO_2 storage during huff-n-puff, and further illustrates the influences of soaking time and injection pressure. Results indicate that CO_2 huff-n-puff significantly mitigates the adverse effects of heterogeneity. The primary cause of residual oil formation is insufficient displacement energy to overcome various flow resistances. CO_2 primarily exists in pore throats as bubbles and is stored in dissolved form in the oil and water phases. As the soaking time and injection pressure increase, the proportion of continuous residual oil decreases noticeably, leading to a higher oil recovery factor. When the injection pressure exceeds the minimum miscible pressure (MMP), the diffusion coefficient of CO_2 increases significantly. Moreover, the presence of vertical fractures effectively expands the diffusion range of CO_2. These findings provide a theoretical basis for the applications of carbon dioxide enhanced oil recovery (CO_2 EOR) and carbon capture, utilization, and storage (CCUS) technologies.

1. Introduction

Despite the gradual increase in the development and utilization of renewable energy, the current global energy consumption is still dominated by fossil energy (British Petroleum, 2020). Lobal energy transition faces numerous challenges, as many countries are heavily dependent on traditional energy sources yet must also consider the costs of usage and potential environmental issues (Guo et al., 2022; Smirnova et al., 2021). In recent years, the urgency to mitigate global warming has become critical, and carbon capture, utilization and storage (CCUS) has been proven to be an effective carbon emission reduction technology (Al-Khdheeawi et al., 2018; Chen et al., 2024; Greig and Uden, 2021; Lv et al., 2022; Wu et al., 2022; Zhang et al., 2024). The utilization of CO_2 for enhanced oil recovery not only secures energy supply and alleviates the pressures of the energy transition, but also contributes to achieving carbon neutrality (Liang et al., 2024).

Heterogeneity exists in strata from micro-to macro-scale (Chang et al., 2016; Jayne et al., 2019). Fractures are common geological structures in strata and play a significant role in oil and gas flow. Heterogeneity and fractures can cause the injected fluid to form preferred flow paths, which significantly affects the overall behavior of fluids in the reservoir (Doughty and Pruess, 2004). Conventional production methods, such as waterflooding and gas displacement, mainly mobilize crude oil in the high permeability region and produce less oil in the low permeability region, which is accompanied by serious water channeling and gas channeling, and the displacement efficiency is not ideal (Fang et al., 2022; Zhong et al., 2022). Due to the strong diffusion and dissolution

* Corresponding author.
E-mail address: cy375@upc.edu.cn (C.-J. Yao).
Peer review under the responsibility of China University of Petroleum (Beijing).

https://doi.org/10.1016/j.petsci.2026.03.014

ability of CO_2, it can reduce the viscosity of crude oil, extract light components and reduce the interfacial tension, and is regarded as a good displacement medium (Huang et al., 2022; Li et al., 2021; Luo et al., 2022; Song and Yang, 2017; Wei et al., 2019). Continuous CO_2 displacement and CO_2 huff-n-puff are two common modes of CO_2 EOR in the petroleum industry, and many studies have shown that the recovery factor of CO_2 huff-n-puff is higher than that of continuous CO_2 displacement (Sheng, 2017; Zuloaga et al., 2017). The process of CO_2 huff-n-puff involves not only the problem of multiphase flow, but also the physicochemical reaction during immersion (Zhang et al., 2019a, 2019b).

In the past few years, a large number of core scale and field scale studies have provided important insights into CO_2 huff-n-puff (Li et al., 2018; Tang and Sheng, 2022; Zhao et al., 2020). However, due to the limitation of traditional experimental methods, the mechanism of fluid transport and migration at pore scale cannot be directly observed. In recent years, the microfluidic technology has advantages in studying the microscopic fluid flow and has gradually matured in the application of CO_2 injection for enhanced oil recovery and CO_2 storage (Huang et al., 2020; Qiu et al., 2021).

In recent years, scholars have conducted a series of microscopic visualization studies of CO_2 in heterogeneous fractured reservoir conditions. Guo et al. (2022) designed a two-permeability microscopic model to simulate the heterogeneous fracture networks and directly observed the fluid behavior during CO_2 huff-n-puff and displacement using microfluidics and fluorescence microscopic imaging. They discovered that miscible CO_2 injection can eliminate the capillary forces under immiscible conditions, promoting film-like displacement, while bubble nucleation, expansion, and migration are the primary driving forces during the huff-n-puff process. Al-Khdheeawi et al. (2017) compared the CO_2 plume migration patterns and trapping mechanism under uniform and non-uniform permeability and porosity distributions. They found that reservoir heterogeneity inhibited the vertical CO_2 migration while promoting horizontal migration. Nguyen et al. (2018) investigated the oil recovery mechanisms of two typical fracture networks: connected and dead-end. They found that bubble nucleation, growth, coalescence, and connected gas flow are the primary mechanisms of oil displacement in fracture networks, noting that connected fractures provide more oil migration paths than dead-end fractures. Zhang et al. (2023) investigated the interaction processes between miscible and immiscible gases and crude oil in deep heterogeneous reservoirs, summarizing the gas displacement mechanisms as immiscible displacement, swelling, and extraction, and evaluating the feasibility of storing CO_2 in deep reservoirs. Liu et al. (2016) investigated the flow of CO_2 and water in heterogeneous pore structures at room temperature and atmospheric pressure, and developed a new parameter, S_{eval}, to characterize the variations in CO_2 saturation. These microfluidic studies have provided detailed analyses ofCO_2 flow in pores and EOR mechanism, offering valuable insights. However, most of these studies considered heterogeneity and fractures separately, without systematically analyzing the migration processes of CO_2, oil, and water migration or the mechanisms of residual oil formation where fractures and heterogeneity coexist.

In this study, we innovatively designed a visual chip with heterogeneity and fractures based on the real reservoir pore structure, and studied the three-phase migration process of oil, gas, and water, the oil recovery mechanism, residual oil distribution, and formation mechanism through microfluidic technology and numerical simulation methods. Firstly, under experimental pressure and temperature conditions ($P = 12$ MPa, $T = 40$ °C), qualitative and quantitative analyses were conducted on the recovery factor, residual oil distribution, and formation mechanism in high permeability and low permeability zones for CO_2 huff-n-puff, CO_2 displacement, and water huff-n-puff. Subsequently, we conducted a detailed study of the factors affecting CO_2 huff-n-puff, including the effects of soaking time and injection pressure. Based on the pressure decline method, the diffusion of CO_2 in the experimental oil was investigated, and it was found that the diffusion coefficient increased significantly when the pressure exceeded the minimum miscibility pressure. Finally, the effects of vertical fractures and horizontal fractures on CO_2 huff-n-puff were investigated, and it was found that vertical fractures had stronger pore connectivity. In general, this paper can provide support for the study of multiphase flow at pore scale with heterogeneity and fractures, and provide theoretical basis for the exploitation of heterogeneous reservoirs and CO_2 storage.

2. Materials and methods

2.1. Materials

The materials used in this experiment include simulated oil, simulated formation water, CO_2, and dye. The oil composition is shown in Fig. 1. The experimental oil sample was prepared by mixing crude oil with white oil. At 40 °C, the oil has a viscosity of 5.60 mPa·s and a density of 0.808 g/cm^3. The minimum miscibility pressure (MMP) between CO_2 and the experimental oil is 13.76 MPa. NaCl (3.90 g), $CaCl_2$ (3.05 g), $MgCl_2$ (1.67 g), and KCl (3.17 g) were weighed and mixed with deionized water in a specific ratio to prepare the simulated formation water. The composition of simulated formation water is shown in Table 1, with a total dissolved solids (TDS) of 21,801.64 mg/L. To clearly observe the dynamic migration process of the oil and water phases, oil red O ($C_{26}H_{24}N_4O$) and methylene blue ($C_{16}H_{18}ClN_3S{\cdot}3H_2O$) were used to dye the experimental oil and simulated formation water, respectively. The dyed liquids were then filtered prior use.

2.2. Design and preparation of micromodel

In this study, a two-dimensional glass microscopic model was made based on the characteristic image of the microscopic pore structure of a heterogeneous reservoir observed, as shown in Fig. 2. The model dimensions are 10 mm × 70 mm, with a thickness of 40 mm and an etching depth of 25 μm. The white portions inside the chip represent the matrix, while the black portions are pore throats, with a pore-throat radius of 1–500 μm. The initial wettability of the model is water-wet. A horizontal fracture, approximately 0.1 mm in aperture and 10 mm in length, runs through its

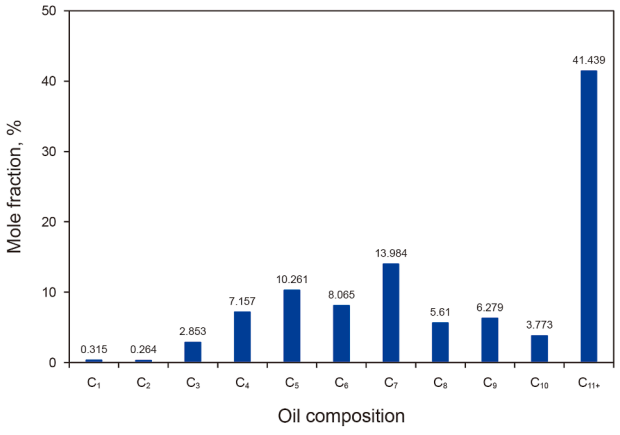

Fig. 1. Composition of the experimental oil.

Table 1
Ionic composition and salinity of the simulated formation water.

Ion concentration, mg/L					TDS, mg/L
Na^+	K^+	Ca^{2+}	Mg^{2+}	Cl^-	
3069.82	3325.20	2202.59	394.88	12,809.15	21,801.64

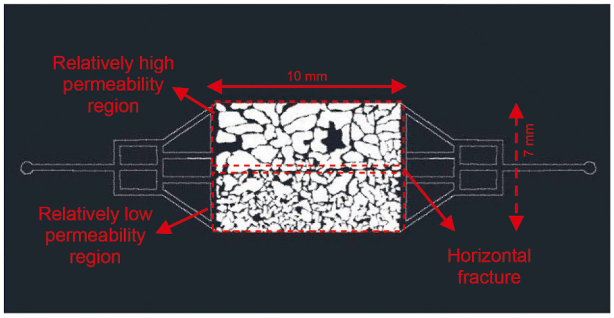

Fig. 2. Schematic diagram of micromodel (microfluidic chip).

center. The pore structures on either side of the fracture are heterogeneous and can be divided into regions of relatively low and high permeability. The overall porosity of the chip is 21.96% and the total pore volume is 3.84×10^{-4} cm^3. The porosity of the relatively high and low permeability regions is 13.1% and 7.89%, respectively, and their pore volumes are 2.29×10^{-4} and 1.38×10^{-4} cm^3.

2.3. Apparatus and procedures

Fig. 3 depicts a high-temperature, high-pressure micromodel apparatus capable of visualizing the CO_2 huff-n-puff displacement process under a range of temperature and pressure conditions. The apparatus mainly consists of an ISCO pump, an integrated control system, a visualization chamber, a microfluidic chip model, a data acquisition system, and a back pressure system. The injection pump is used primary for water injection to drive the piston within the intermediate container, thereby injecting fluid from the intermediate container into the chip. The function of the confining pump is to apply the confining pressure to the chip and simulate the overburden pressure of the formation. The pump operates in tracking mode to maintain the external confining pressure at 3–5 MPa above the internal pore pressure, thereby ensuring the integrity of the chip. The integrated control system features an interactive interface that allows for direct control of the entire system's parameters, including pressure, temperature, and injection rate. There are three intermediate containers that enable heating of the fluid with a precision of 0.1 °C, containing dyed experimental oil, simulated formation water, and CO_2, respectively. Both the upper and lower parts of the visualization chamber are made of transparent, high-pressure-resistant glass, securely holding the chip. The data acquisition system, composed of a high-definition digital camera and a computer, captures fluid flow processes within the chip in real time. Finally, the back-pressure system regulates the outlet pressure to control the production differential pressure.

Fig. 4 shows the experimental apparatus for measuring the CO_2 diffusion coefficient in the oil phase. The device mainly includes a temperature and pressure control box, an intermediate container, an ISCO pump, a diffusion cell, and a vacuum pump. The diffusion cell has an internal volume of 50 cm^3 and a height of 7.08 cm. The temperature and pressure control box can heat the interior of the diffusion cell, with a maximum temperature control of 120 °C. The connected computer can record the pressure changes during the CO_2–crude oil diffusion process.

The procedures for the micromodel simulation are as follows:

(1) The visualization chamber is cleaned with deionized water to ensure cleanliness and the system temperature is set to 40 °C.
(2) With formation-water and outlet valves opened, formation water is injected at a rate of 0.01 mL/min until the chip is fully saturated. The formation-water valve is closed and the simulated oil is injected to displace the water. Injection stops when the oil–water distribution stabilizes, and the system is left to stand for 12 h.
(3) CO_2 is injected into the chip and soaked for 15 min. The injection-end valve is then reopened to initiate oil production. The three-phase flow is monitored in real time via the data acquisition system.

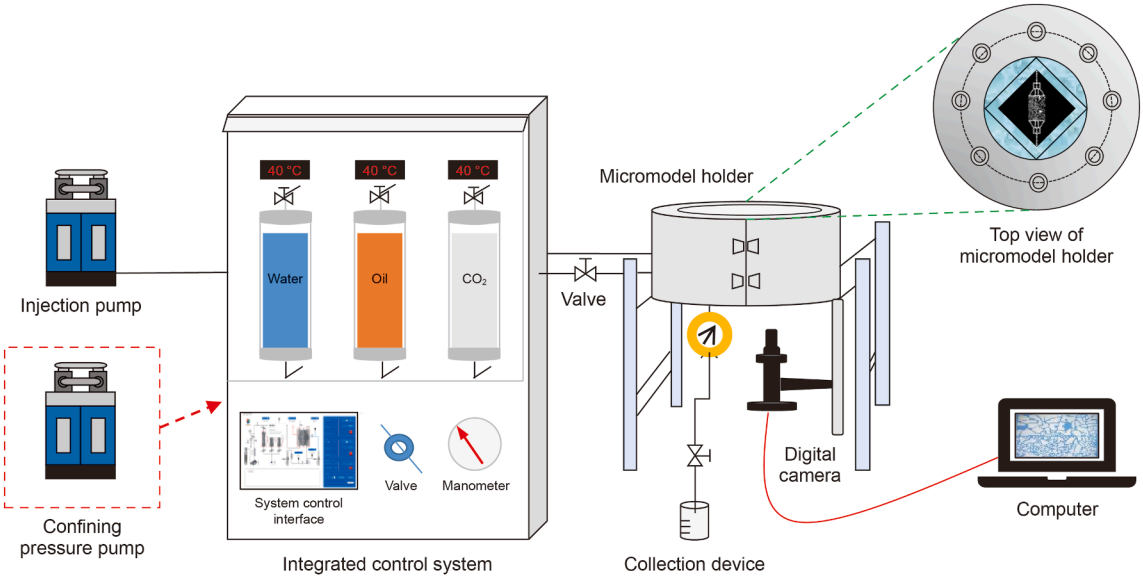

Fig. 3. High-temperature, high-pressure micromodel apparatus for visualizing CO_2 huff-n-puff.

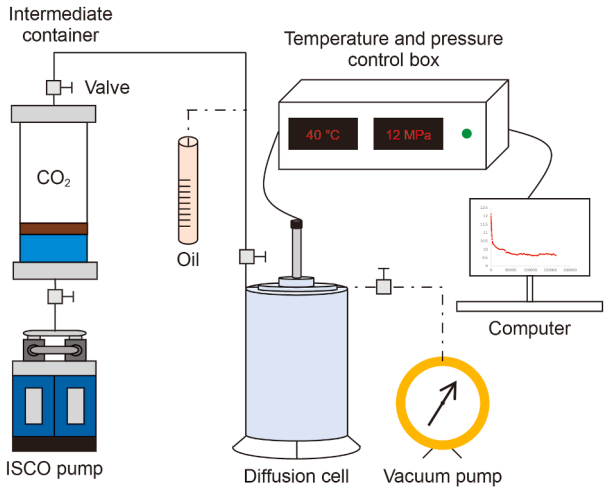

Fig. 4. Experimental apparatus for measurement of CO_2–oil diffusion.

(4) After the huff-n-puff experiment, the chip is cleaned with deionized water and petroleum ether, and then re-saturated with oil and water (as in Step (2)). Water huff-n-puff experiments follows the same step as CO_2 huff-n-puff (as in Step (3)). CO_2 displacement also occurs at 12 MPa for 15 min. The difference with huff-n-puff is that the outlet valve is also opened during the oil production process.

(5) Then the chip is cleaned and then saturated with oil and water. CO_2 injection pressure (12, 18, 24, 30 MPa) and soaking time (15, 30, 45, 60 min) are systematically varied for the subsequent production tests. After the experiment, the acquired images are analyzed by professional software. It is worth noting that the above oil production process is carried out at 4 MPa.

In the CO_2–oil diffusion experiment, the gas tightness of the device should be checked first. The diffusion cell is evacuated for 12 h until the internal pressure reaches −0.1 MPa. If the pressure change is less than 0.01 MPa after 30 min, the internal gas tightness is considered satisfactory. After evacuation, the valve at the left end of the diffusion cell is opened, allowing oil to enter the diffusion cell under the pressure differential. The temperature of the diffusion cell is controlled at 40 °C. Subsequently, the intermediate container containing CO_2 is opened, and CO_2 is injected into the diffusion cell using a displacement pump until the preset experimental pressure (12–30 MPa) is reached, and the pressure setting is synchronized with the microscopic visualization experiment. Finally, the valve is closed, the pressure change data in the diffusion cell is recorded.

2.4. Image analysis

In order to quantitatively characterize the oil migration and residual oil distribution, Image-Pro Plus software is used to perform color threshold segmentation on the experimental images. This method directly distinguishes oil and water phases based on color difference and calculates the area of each phase. As shown in Fig. 5, the oil and water phases are identified and marked with green and blue, respectively. Subsequently, the residual oil area and recovery factor are calculated. The calculation equations are detailed below.

$$R_o = \frac{S_{o1} - S_{o2}}{S_{w1} + S_{o1}} \tag{1}$$

$$R_r = \frac{S_{or}}{S_{w1} + S_{o1}} \tag{2}$$

$$R_l = 1 - \frac{S_{o2} + S_{w2}}{S_{w1} + S_{o1}} \tag{3}$$

where R_o is the recovery factor; S_{o1} is the area of the initial saturated oil; S_{o2} is the oil phase area after production; R_r represents the proportion of a certain type of residual oil; S_{or} is the residual oil area; S_{w1} is the initial saturated water area; R_l is the liquid recovery factor; S_{o2} and S_{w2} represent the areas of oil and water after production, respectively.

2.5. Calculation method of CO_2–oil diffusion coefficient

In this paper, the pressure drop method proposed by Zhang et al. (2000) is used to determine the diffusion coefficient of CO_2 in oil under different pressures. The specific method for calculating the diffusion coefficient is as follows:

$$P(t) - P_{eq} = \frac{8BLC_{eq}}{\pi^2} \exp\left(-\frac{\pi^2 D}{4L^2} t\right) \tag{4}$$

$$\ln[P(t) - P_{eq}] = \ln\left(\frac{8BLC_{eq}}{\pi^2}\right) - \frac{\pi^2 Dt}{4L^2} \tag{5}$$

$$D = \frac{4kL^2}{\pi^2} \tag{6}$$

where D is the diffusion coefficient of the CO_2–oil system, m^2/s; $P(t)$ represents the pressure at any time in the diffusion cell, MPa; P_{eq} is the pressure after reaching equilibrium, MPa; L is the height of the oil in the diffusion cell, m; k is the slope of the curve for the logarithm of pressure difference versus time.

2.6. Simulation

2.6.1. Simulation model

Based on the chip model designed in the previous stage, two numerical models with local characteristics of the chip were established using COMSOL Multiphysics, as shown in Fig. 6. The white part of the model represents the matrix and the black part represents the pore throats. These two models are 0.906 mm × 0.54 mm in size, with 127,645 and 121,042 mesh, and porosity of 19.15% and 23.06%, respectively. The radius distribution of pore throats ranges from 0.5 to 200 μm.

The basic parameters of the model are as follows: The boundary conditions at the inlet and outlet are restricted by pressure conditions. The solver uses a time step of 0.0001 s, with a total simulation time of 0.005 s. The system temperatures for both CO_2 and oil are maintained at 40 °C, and the physical property parameters (e.g. oil viscosity) are consistent with the experimental part. The oil–CO_2 contact angle and interface tension are set to 120° and 0.07 N/m, respectively. The interface thickness control parameter ε_{pf} is set to 0.00001 m and the mobility is set to 0.001 (m·s)/kg.

2.6.2. Simulation scheme

This study conducts a comprehensive investigation of heterogeneous fractured reservoirs. In the simulation component, we focus on the characteristics of CO_2 displacement under both conditions with and without fractures. Notably, this simulation

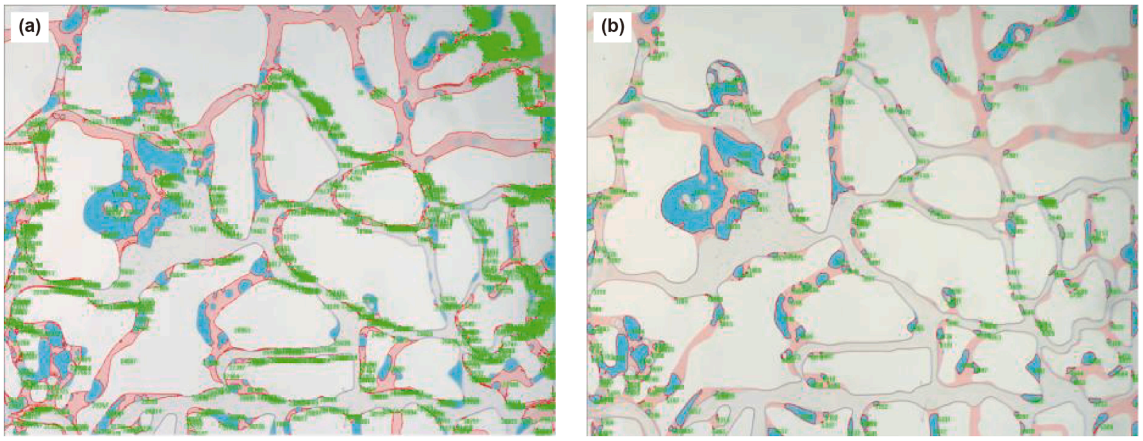

Fig. 5. Delineated area distribution of oil (**a**) and water (**b**) after production.

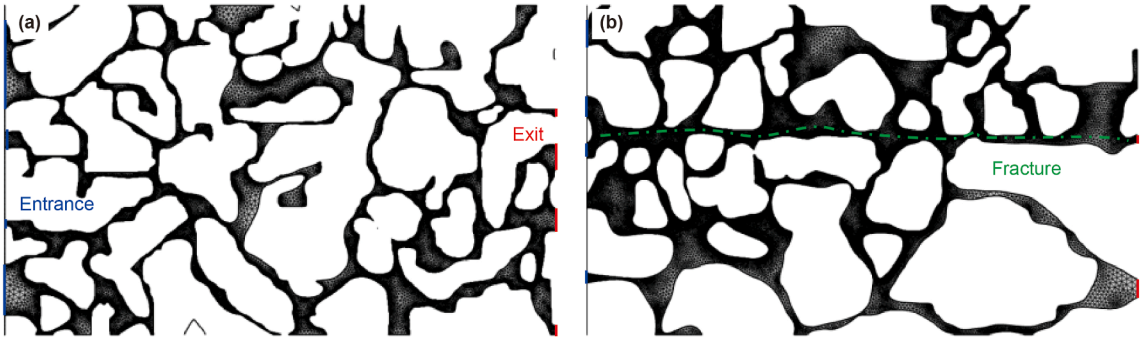

Fig. 6. Microsimulation model without (**a**) and with (**b**) fracture.

scheme differs somewhat from the microscopic physical simulation experiment: the numerical simulation adopts CO_2–oil two-phase flow, whereas the experiment involves oil–CO_2–water three-phase flow. Initially, a three-phase flow model was attempted to replicate the physical experimental conditions. Firstly, the porous medium is saturated with water phase, followed by oil displacement to form the initial oil–water distribution. However, because the mathematical model in the simulation software relies on simplified parameters, discrepancies with actual fluid flow behavior arose. Specifically, this resulted in the almost complete expulsion of pore water, rendering the subsequent CO_2 huff-n-puff process effectively a two-phase interaction. Therefore, a CO_2–oil two-phase system was adopted for the subsequent simulation work in this paper.

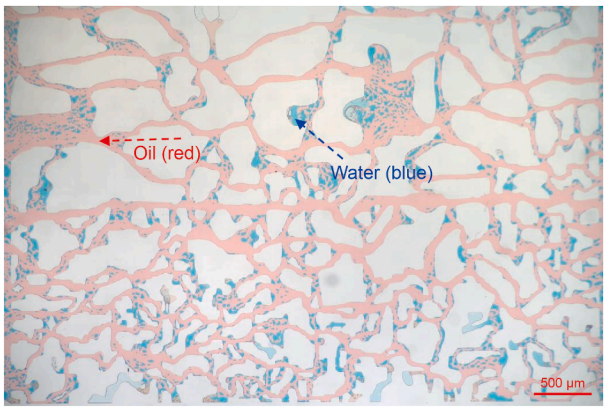

Fig. 7. Initial oil–water distribution.

3. Results and discussion

3.1. Analysis of displacement mechanisms of different production methods

In order to clarify the oil displacement characteristics of CO_2, the results obtained at an injection pressure of 12 MPa and immersion time of 15 min were compared with those from 15 min water huff-n-puff and continuous CO_2 displacement experiments. Fig. 7 shows the initial oil–water distribution of the chip. The initial oil saturation of the chip is 82.68% and the initial water saturation is 17.32%.

The production efficiency under the three production methods was quantitatively analyzed, and the results are shown in Fig. 8. The liquid recovery of CO_2 displacement, water huff-n-puff, and CO_2 huff-n-puff reached 56.44%, 61.4%, and 65.31%, respectively. The oil recovery factor under CO_2 huff-n-puff is observed to be 11.78% and 13.25% higher than that achieved by CO_2 displacement and water huff-n-puff, respectively. Water huff-n-puff had the highest water recovery factor, reaching 20.05%. Analysis indicates that CO_2 exhibits a distinct advantage over water in diffusion and dissolution, which is significant for efficient oil production (Liu et al., 2023; Rossen, 2017; Sun et al., 2019). Fig. 8(b) shows the production contributions from different regions under the three production methods. Comparing CO_2 displacement with CO_2 huff-n-puff, the contribution rate of recovery factor in the high permeability area decreased gradually from 69.31% to 54.1%.

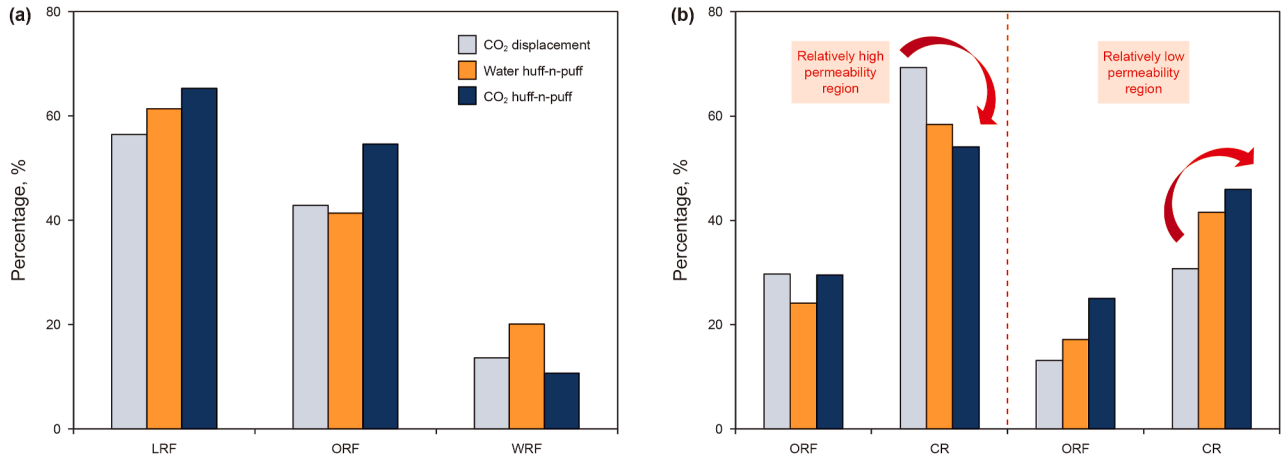

Fig. 8. Comparison of recovery factor for different production methods. (**a**) Liquid recovery factor (LRF), oil recovery factor (ORF), and water recovery factor (WRF) of CO_2 displacement, water huff-n-puff, CO_2 huff-n-puff; (**b**) ORF and contribution rate (CR) in high permeability and low permeability regions.

However, in the relatively low permeability region, it gradually increased from 30.69% to 45.9%. This variation in recovery contributions indicates that given reservoir heterogeneity, gas flooding primarily mobilizes oil in high permeability regions, while huff-n-puff achieves more balanced production across different regions. Owing to heterogeneity, significant differences in pressure propagation and gas concentration exist between high and low permeability regions. During the soaking stage, driven by concentration and pressure gradients, CO_2 diffuses extensively into low permeability regions, interacting fully with the oil.

The experimental results show that the residual oil can be divided into five types: columnar, single-pore, porous, membranous, and cluster (Lei et al., 2022). In this paper, the porous and cluster residual oil are classified as continuous oil. This type of residual oil features a large contiguous area, good continuity, and significant potential for enhanced recovery. The remaining three types are categorized as discontinuous, characterized by their small scale and isolated distribution, making them difficult to mobilized. Fig. 9 shows the formation mechanism of different types of residual oil. Columnar residual oil is the most common form, and it is easy to form in the throat which is nearly perpendicular to the displacement direction. Two pressure values with opposite directions but similar magnitudes are present on either side of the throat. Consequently, the resulting pressure gradient is insufficient to mobilize this portion of the oil. Single-pore residual oil is generally formed in isolated pores, and the connectivity between isolated pores and main seepage channels is poor. On the one hand, it is difficult for displacing fluid to spread into the oil phase in the pores; on the other hand, due to hydrophilic nature of the pore walls, capillary forces act as a resistance in the process during gas displacement. Moreover, the radii of isolated pores are relatively small, resulting in high capillary force. The displacement force P of the liquid is insufficient overcome the capillary force required to mobilize the fluid. The porous residual oil is mainly formed between two or more pore throats, characterized by continuity and wide distribution. The pore space formed by the connection of multiple throats exhibits high tortuosity, resulting in significant resistance to the flow of oil. The residual oil in membranous form is common on the concave or convex surface of the pore wall with a specific curvature, featuring small area and wide distribution. Strong adhesive forces exist between the oil film and the pore wall, making it difficult for displacing fluid to detach it. The cluster residual oil is distributed continuously in bulk, accompanied by oil–water mixing. At the intersection of pores and throat, due to the strong resistance to liquid beads caused by the Jamin effect, the oil phase remains trapped in the pores and cannot migrate through the throat. If there is not enough energy, liquid beads will gather in the pores to form clusters of residual oil.

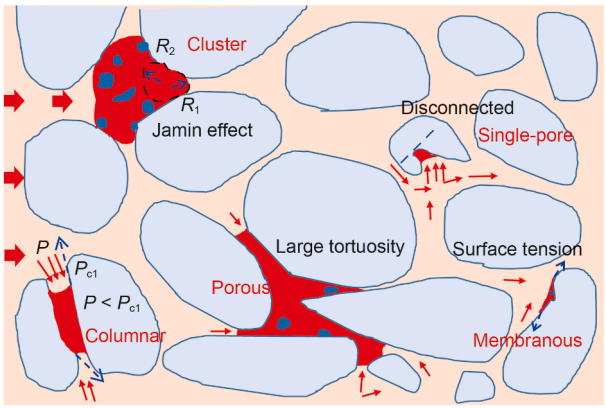

Fig. 9. Schematic diagram of formation mechanism of different types of residual oil.

The distribution of residual oil in the relatively low and high permeability regions after CO_2 displacement, water huff-n-huff, and CO_2 huff-n-puff is shown in Fig. 10. In Fig. 10, the blue, green, pink, yellow, and black dotted areas delineated respectively represent columnar, single-pore, porous, membranous, and cluster residual oil. By comparing areas 1, 2, and 3, it can be observed that for the same area, different production methods and media have significant impacts on the type of residual oil formed. Taking area 1 as an example, after CO_2 huff-n-puff and water huff-n-puff, a smaller area of membranous residual oil was formed at this location, while CO_2 displacement resulted in a larger area of porous residual oil. Results indicates that after CO_2 displacement, the residual oil in the high permeability region is mainly columnar and single-pore, whereas in the low permeability region, it is mainly porous and cluster. A significant amount of CO_2 escapes along the fracture, resulting in limited CO_2 sweep range. The red arrow in Fig. 10(a) indicates the main direction of CO_2 flow. Oil within the CO_2 flow channel is mostly displaced, while the surrounding oil remains poorly mobilized. It is evident that the residual oil concentrates in the edge area distal from the fracture. During the soaking stage, driven by internal pressure difference, the sweep

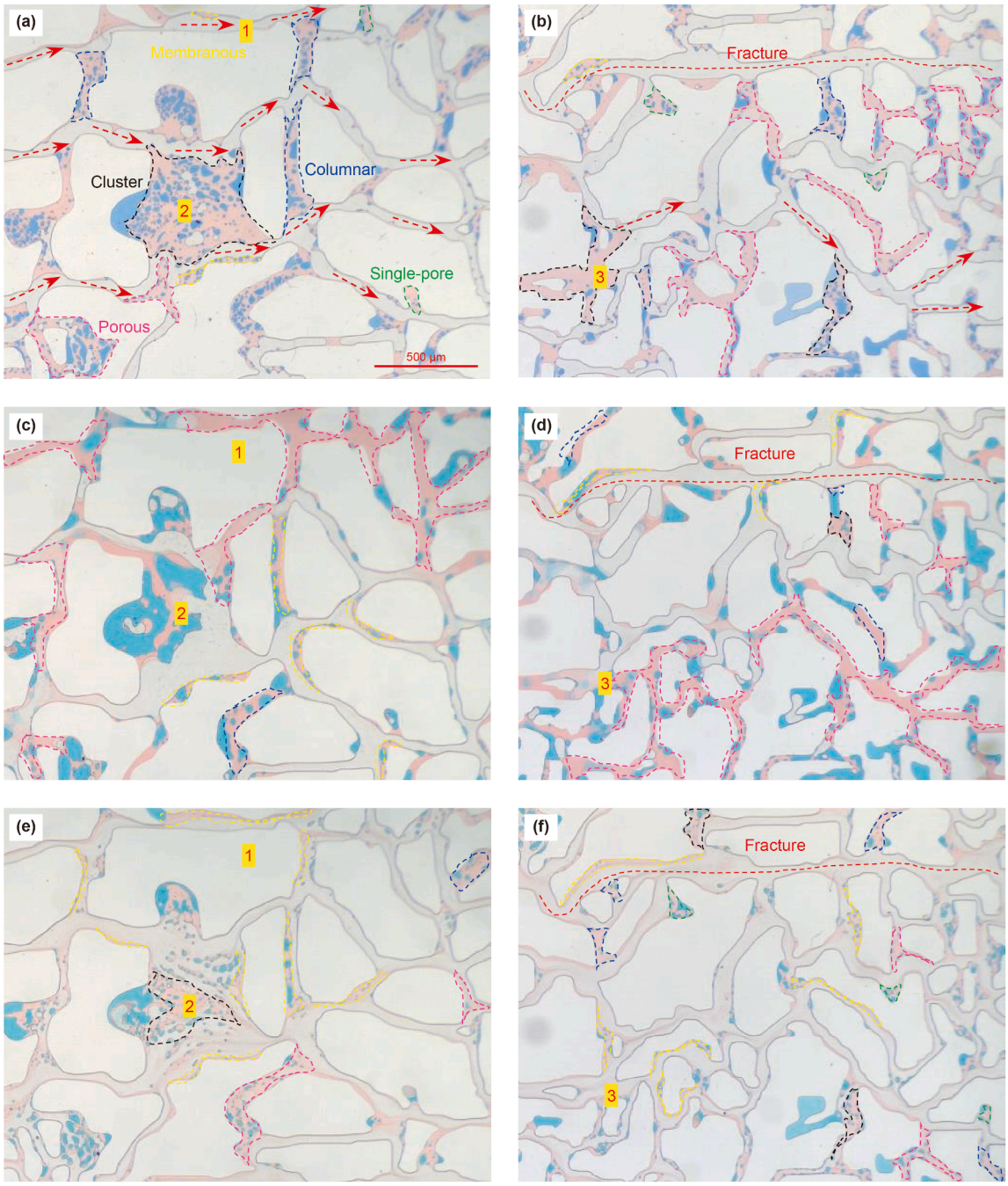

Fig. 10. Distribution of residual oil after displacement by different production methods. CO_2 displacement in high (**a**) and low (**b**) permeability regions; water huff-n-puff in high (**c**) and low (**d**) permeability regions; CO_2 huff-n-puff in high (**e**) and low (**f**) permeability regions.

efficiency of the medium in the low permeability region gradually expands, the pressure distribution is gradually uniform, and the adverse influence of reservoir heterogeneity is weakened. Due to the hydrophilic characteristics of pore wall, pronounced spontaneous imbibition occurs during water huff-n-puff, and the capillary force aids oil recovery. Due to its inherent characteristics, CO_2 exhibits vigorous diffusion during the soaking stage, and a substantial amount dissolves in the oil phase, resulting in viscosity reduction, volume expansion, and energy increase. A significant quantity of oil in the low permeability region is produced, and a lightening of the oil phase color was observed (Abedini et al., 2014; Alfarge et al., 2017; Ghasemi et al., 2017). In addition, the experiment shows that the oil in the pores around the fractures is usually displaced into the fracture for migration with only a small amount of membranous residual oil remaining in the fracture.

The distribution of different types of residual oil in high and low permeability regions was quantitatively characterized by micro-displacement experiments under different production methods. As shown in Fig. 11, the production method has a significant impact on the residual oil saturation and the proportion of different types of residual oil. The effective swept area of CO_2 huff-n-puff in the low permeability region is 11.99% higher than that of CO_2 displacement. After CO_2 huff-n-huff, the proportion of continuous residual oil is 9.74% less than that of displacement,

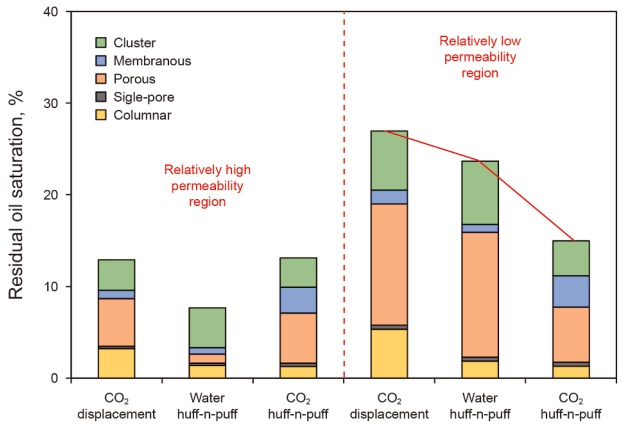

Fig. 11. Residual oil saturation after displacement by different production methods.

while the discontinuous residual oil significantly increases. Analysis indicates that CO_2 huff-n-huff can effectively reduce the influence of reservoir heterogeneity than CO_2 displacement. Driven by pressure differentials and fractures in pores, the gas has a wider diffusion range, and enhanced physicochemical interactions with oil phase occur. In addition, the proportion of residual oil varies with different huff-n-puff media. The continuous residual oil after water huff-n-puff is 17.37% more than that after CO_2 huff-n-puff. The spread range of CO_2 in the low permeability region is 8.7% higher than that of water. Analysis suggests that CO_2 is in a supercritical state at 40 °C and 12 MPa (Ding et al., 2021). It combines the strong fluidity of liquid and the strong diffusivity of gas. Consequently, its migration capacity in the pore throat is stronger than that of water, and it can dissolve in the oil phase, targeting large-scale continuous residual oil more effectively than water.

3.2. Analysis of influencing factors of CO_2 huff-n-puff

3.2.1. Influence of soaking time

Soaking time has a significant effect on the distribution of residual oil and water in pores. Fig. 12 shows the distribution characteristics of oil and water in the pore throats after different soaking time. As shown in Fig. 12(a), when the soaking time increased from 15 to 60 min, CO_2 bubbles were observed within the oil phase in isolated pores, fragmenting the continuous oil phase, which, however, remained trapped. With the increase in soaking time, the oil phase in the macropores became more dispersed, and the phase boundaries grew more distinct. The membranous residual oil in the throat transformed into shorter columnar residual oil, and almost all the membranous residual oil in the fracture was mobilized. The oil phase, which had less connected with water in the pore throat near the fracture, was eventually able to migrate along the fracture. It can be seen from Fig. 12(b) that the residual oil at the edge of the low permeability region could also be effectively used with the increase in soaking time. The analysis shows that a longer soaking time results in a wider CO_2 diffusion range. When CO_2 displaces oil into the bellowing channel, it is easy to merge with the original film-like residual oil there. This makes the oil area larger, generates large capillary forces on both sides of the bellowing channel, and has limited displacement energy itself, resulting in the oil phase staying in the bellowing channel and forming new columnar residual oil. The soaking time mainly affects the migration of the oil phase that is not in close contact with water. For oil phase with extensive water contact, the migration range is limited due to high resistance and low displacement energy. In addition, water can also dissolve CO_2, thereby reducing the amount of CO_2 available for diffusion into the oil.

Fig. 13 shows the recovery factor and residual oil distribution after CO_2 huff-n-puff under different soaking time with injection pressure of 12 MPa. The oil recovery factor increased significantly from 15 to 30 min, with an increasement of 8.08%. However, when the soaking time was extended from 45 to 60 min, the recovery factor increased by only 1.67%, reaching 67.79%. It can be seen that once the soaking time exceeded 45 min, the impact on the recovery factor diminished. In addition, the proportion of continuous residual oil (porous and cluster types) decreased by 2.91% from 30 to 45 min, and only 1.77% from 45 to 60 min, leaving only 4.92% at 60-min soaking time. Consequently, the potential for further recovery was greatly reduced. Therefore, 45 min is considered the optimal soaking time.

Simultaneously, it can be observed that as the soaking time increased, the proportions of cluster, membranous, and porous residual oil decreased, while the proportion of columnar residual oil gradually increased, and the proportion of single-pore residual oil remained largely unchanged. The analysis indicates that with the increase in time, sufficient diffusion and mass transfer occur between CO_2 and oil, which has a significant mobilization effect on continuous residual oil distributed in various pores in both high and low permeability regions. CO_2 diffuses into the oil, causing it to expand in volume and decrease in viscosity. Meanwhile, some of the light components also diffuse into the free CO_2 and are subsequently carried out of the pores. With prolonged soaking time, the oil displacement efficiency does not increase indefinitely. After reaching a certain extent, the influence of soaking time on the oil–gas–water flow gradually diminishes. However, if the displacement pressure in pores can be effectively replenished, the residual oil can be further mobilized.

3.2.2. Influence of injection pressure

Pressure serves as the driving force for the migration of oil, gas, and water in porous media, and then injection pressure has an important effect on the behavior of the three-phase flow. To investigate the influence of injection pressure, CO_2 huff-n-puff displacement experiments were conducted at a fixed soaking time of 30 min. The three-phase flow mechanisms at different pressures are shown in Fig. 14.

At an injection pressure of 12 MPa, the oil–water mixture remained immobilized in the throats, the oil in the isolated pores was unswept, and the oil at the edges of low permeability regions exhibited limited mobility. As the pressure continued to rise, the solubility of CO_2 in oil improved, the color of the oil phase became obviously lighter, a large area of CO_2 bubbles appeared in the isolated pores, and a large amount of residual oil was effectively produced through the columnar residual oil flow in the pore throat around the fracture. The oil phase in the low-permeability edge region remained largely immobile. It can be observed from Fig. 14 that after the pressure reached 30 MPa, almost all the residual oil was dispersed.

The analysis shows that the change of oil–gas–water three-phase flow with pressure is a complicated process. At low injection pressure, when gas encounters multiple throats while displacing the oil phase, it preferentially flows through the channels offering lower resistance, rather than entering pathways characterized by extensive oil–water distribution. As the pressure gradually increases, this selective behavior diminishes, and sufficient energy becomes available to overcome the resistance in adjacent throats, thereby displacing the oil and water phases. The oil phase within the throats is typically adsorbed along the pore walls on both sides of the migration path. The principal direction of the applied pressure aligns with the orientation of the throat. When

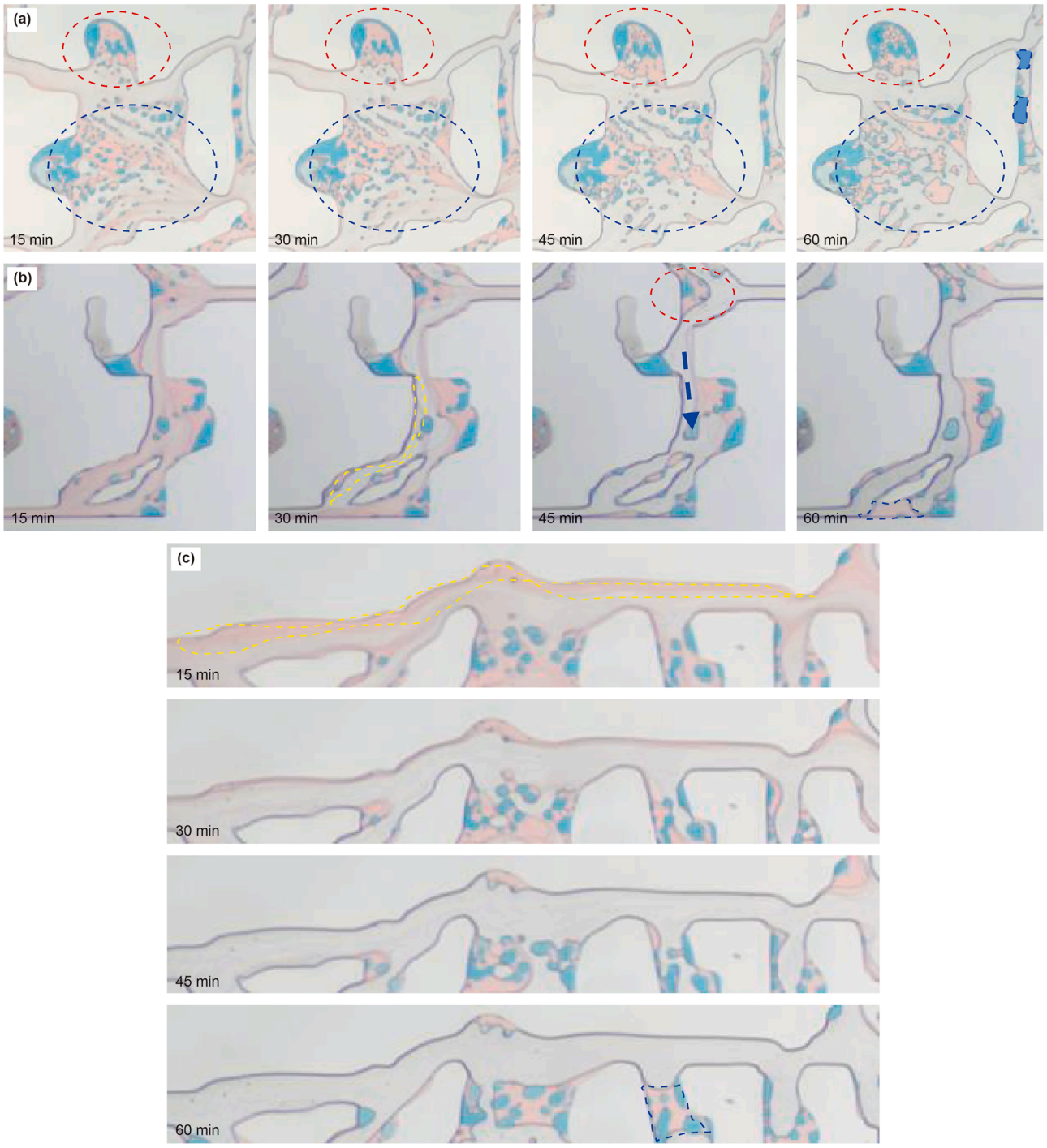

Fig. 12. Distribution characteristics of oil, gas, and water after different soaking time. (**a**) High permeability region; (**b**) low permeability region; (**c**) fracture.

moving from the throat into the pore, the direction and magnitude of the pressure are influenced by the throats connected to that pore, resulting in force components in multiple directions. Along the migration path of the oil phase, the pressure gradually decreases, eventually allowing the oil phase to be distributed freely within the pore-throat network.

When the injection pressure exceeds the MMP of 13.76 MPa, the interfacial tension between CO_2 and oil almost disappears, the diffusion of gas to oil increases, the oil phase expands, and the elastic energy increases. In addition, it is observed that the final residual oil is basically distributed in the marginal zone away from the fracture. This can be explained for three reasons. Firstly, the energy is insufficient when CO_2 propagates into the edge region. Secondly, the horizontal fracture configured inside the chip provides limited influence; the effect of vertical fractures will be investigated in subsequent studies. Thirdly, the closed boundary condition at one end hinders fluid flow.

Fig. 15 shows the distribution and recovery factor of residual oil in high and low permeability regions following CO_2 huff-n-puff under varying injection pressures. When the pressure increased

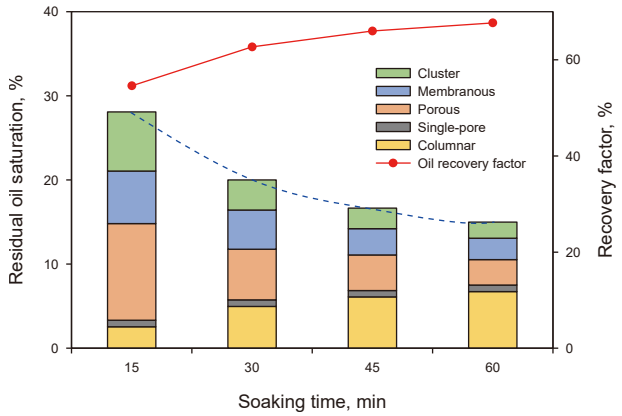

Fig. 13. Recovery factor and residual oil distribution after different soaking time.

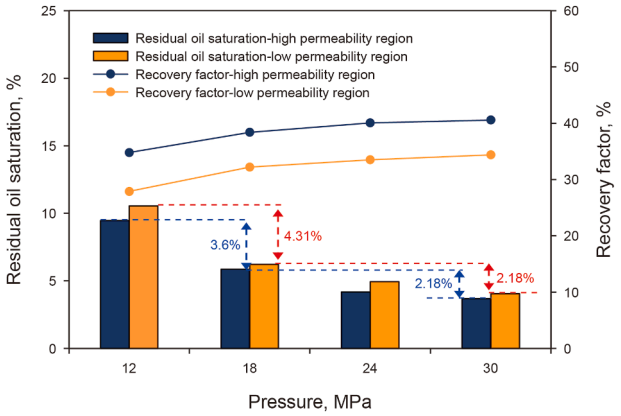

Fig. 15. Distribution of residual oil and oil recovery factor after CO_2 huff-n-puff under different injection pressures.

from 12 to 18 MPa, and the recovery factors in high and low permeability regions increased by 3.6% and 4.31%, respectively. With a continuous pressure increase to 30 MPa, the total recovery factor of high and low permeability regions reached 74.95%, but the changes of residual oil and recovery decreased. The experimental results show that the production degree of CO_2 and oil in the miscible state is superior to that in the immiscible state, but the influence of the increase in pressure on the oil phase flow will be weakened when the pressure exceeds the miscible pressure.

Diffusion is a fundamental mechanism driving oil phase expansion, energy enhancement, and oil viscosity reduction induced by CO_2 during the soaking stage. Fig. 16 presents the diffusion coefficient of CO_2 in the oil phase under different pressure conditions, with detailed pressure variation data inside the

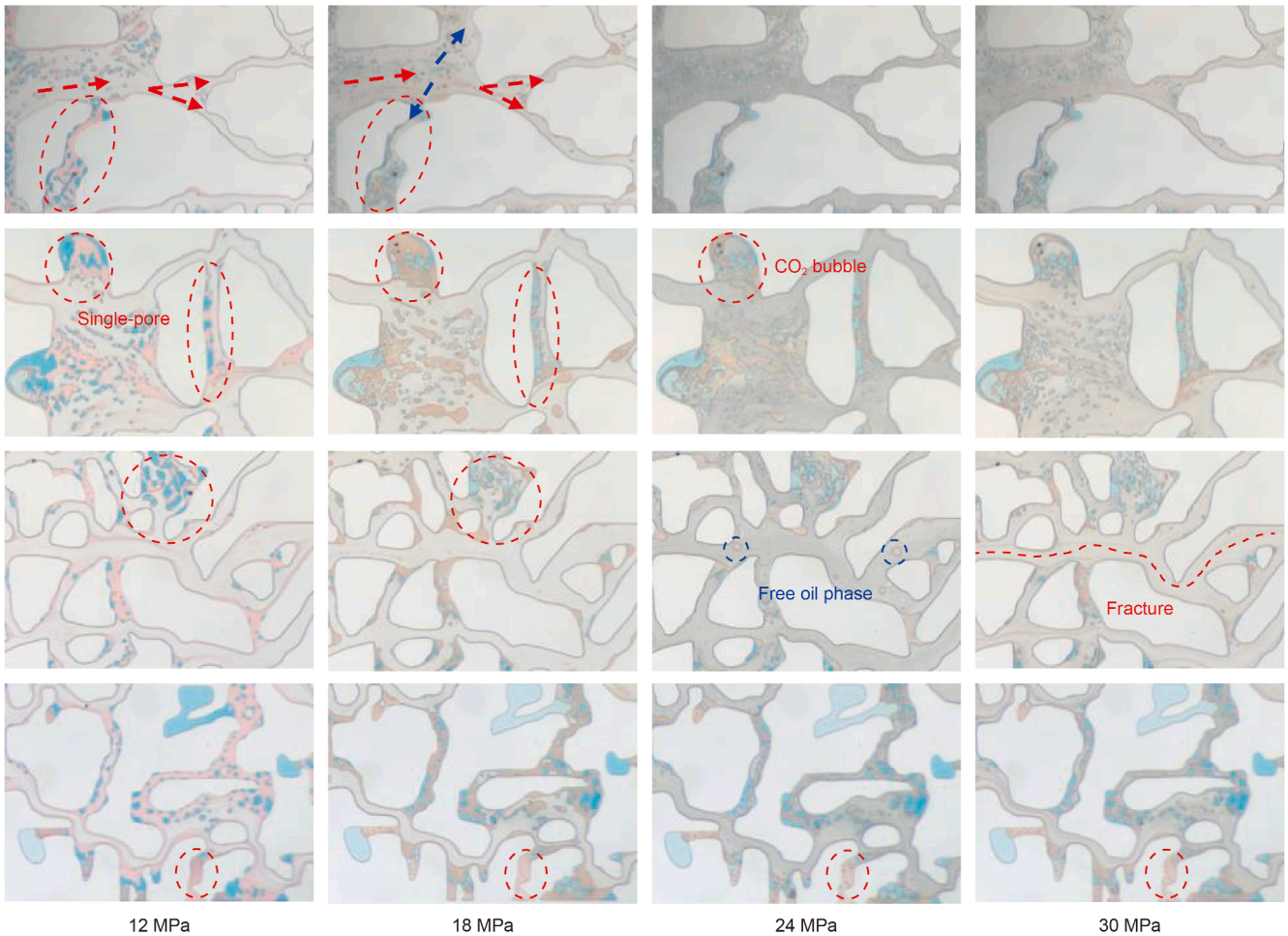

Fig. 14. Three-phase migration mechanisms under different injection pressures.

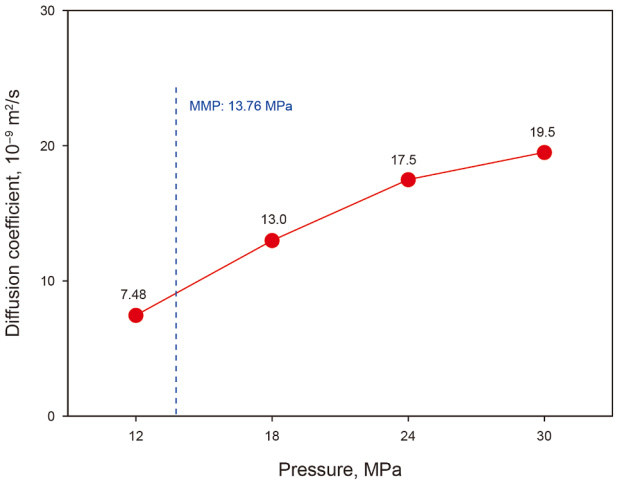

Fig. 16. Diffusion coefficients of CO_2–oil under different pressures.

diffusion cell provided in the Appendix A. The diffusion coefficient of CO_2 in the experimental oil ranged from 7.48×10^{-9} to 19.5×10^{-9} m^2/s. When the pressure increased from 12 to 18 MPa, the diffusion coefficient increased by 5.52×10^{-9} m^2/s, and the change amplitude is the largest at this time. When the pressure exceeded 18 MPa, the rate of increase of the diffusion coefficient diminished. Based on the pressure variations in the diffusion cell, the diffusion process is categorized into three stages: rapid diffusion, slow diffusion, and equilibrium. The diffusion coefficient calculated in this study is the average value of the whole diffusion process, rather than the coefficient for a specific stage. The experimental results demonstrate that the diffusion coefficient of CO_2 in the oil phase increases with increasing pressure. Notably, when the pressure exceeds the miscible pressure, the diffusion coefficient increases significantly. For a constant soaking time, increasing injection pressure can expand the diffusion range of CO_2. Under a constant pressure condition, a longer the soaking time results in a larger diffusion area, thereby enhancing the mobilization of residual oil.

3.3. Simulation results of CO_2 huff-n-puff under different parameters

3.3.1. Influence of diffusion coefficient on displacement

Based on the diffusion coefficient measured in the previous experiment, it is found that the influence of the experimental diffusion coefficient on the characteristics of CO_2 displacement is not significant. Fig. 17 illustrates the oil displacement characteristics of CO_2 in porous media with a diffusion coefficient ranging from 2.54×10^{-7} to 2.54×10^{-10} m^2/s. In the initial state, the pore oil saturation is 100%, and the color strip reflects the variations in CO_2 concentration. As observed from Fig. 17, upon entering the oil-saturated porous medium, CO_2 preferentially flows through channels with low resistance, resulting in distinct viscous fingering, which is independent of the diffusion coefficient (Jia et al., 2022). The simulation results show that as the diffusion coefficient increases, the CO_2 displacement front advances more

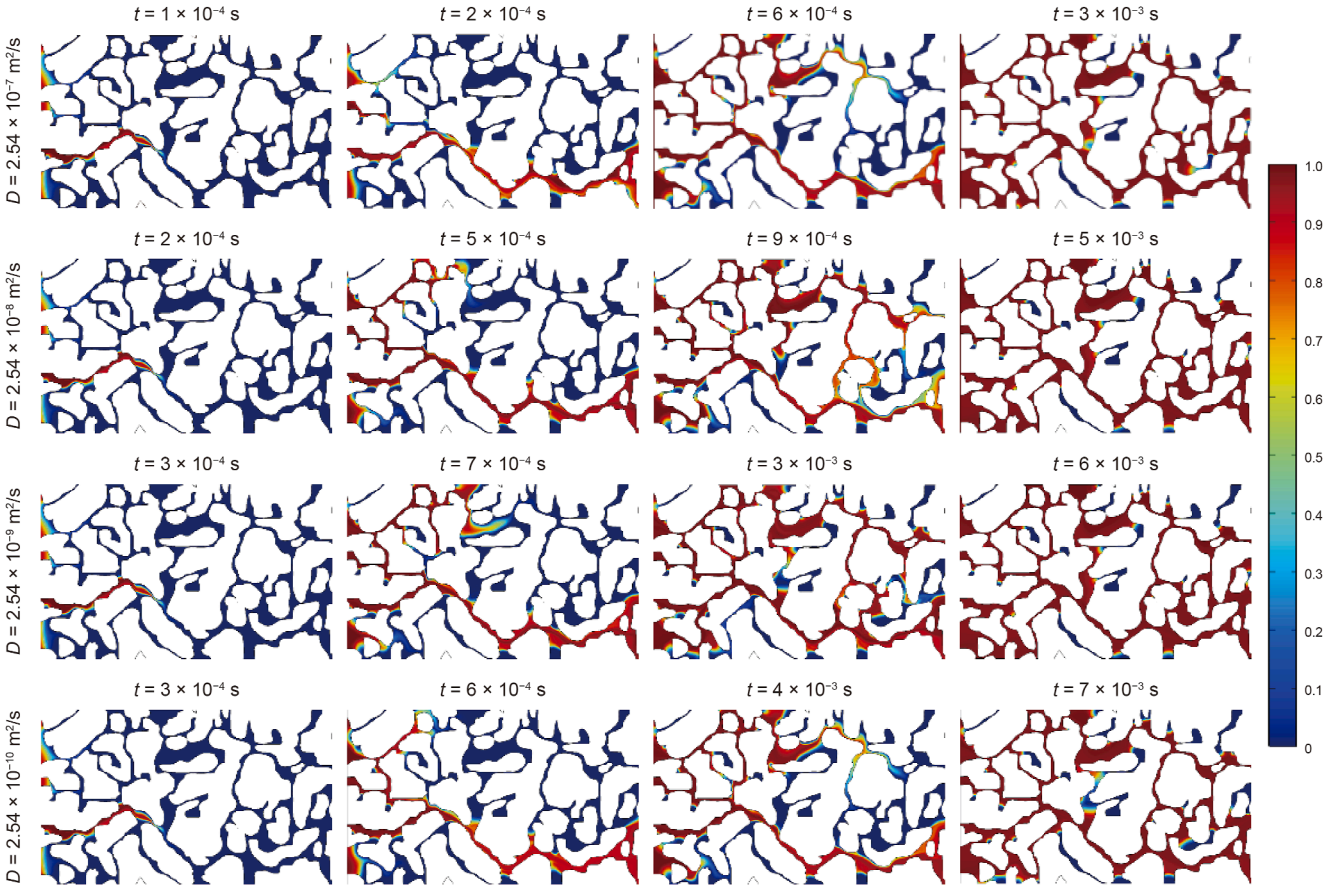

Fig. 17. Displacement characteristics under different CO_2 diffusion coefficients.

rapidly, indicating that within the same timeframe, the greater the diffusion coefficient, the larger the CO_2 sweep range (Seyyedi and Sohrabi, 2020). However, the final residual oil distribution seems to have little relationship with the diffusion coefficient and is primarily distributed in isolated pores and narrow throats. This is because only the diffusion mechanism of CO_2 is considered in the simulation process, given sufficient time, the eventual spread range will reach the same level.

3.3.2. *Influence of fractures on displacement*

In this paper, the effects of horizontal and vertical fractures on CO_2 huff-n-puff displacement at 12 MPa were investigated, and the simulation results are presented in Fig. 18. Upon entering the pores, the gas preferentially displaces the oil phase along the horizontal fracture and subsequently begins to diffuse into the area adjacent to the horizontal fracture. Fig. 19 illustrates that the recovery factor exhibits a rapid increase within 6×10^{-4} s, followed by a gradual rise beyond this time interval, ultimately stabilizing at approximately 5×10^{-3} s. The models incorporating both horizontal and vertical fractures demonstrate recovery factors exceeding 90%, significantly surpassing those observed in the model without fracture.

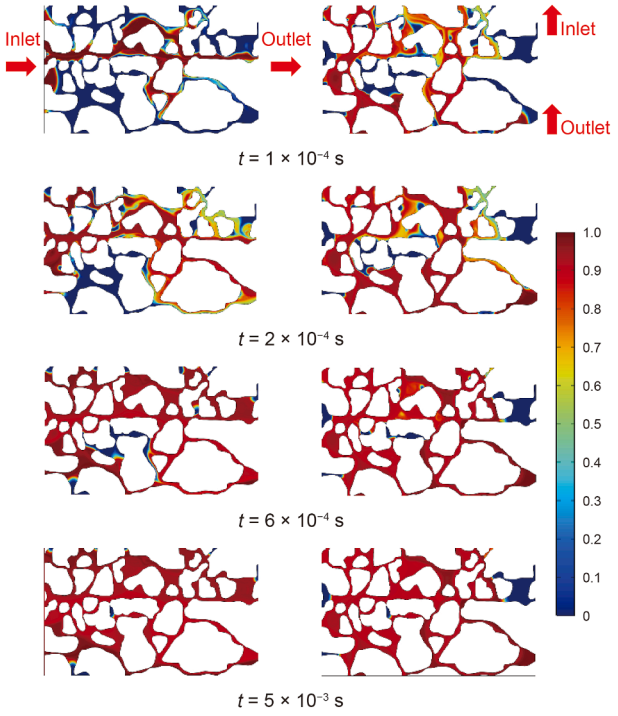

Fig. 18. CO_2 displacement characteristics under horizontal and vertical fractures.

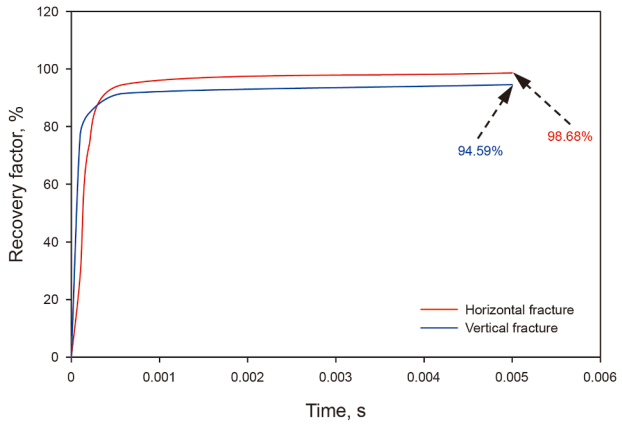

Fig. 19. Variation curves of CO_2 displacement recovery factor under different models.

Interestingly, it was observed that CO_2 initially migrates to the pores near the outlet end, while the oil phase near the inlet end is mobilized later. This phenomenon is attributed to the heterogeneous model configuration, where the pore throat permeability near the exit is higher than that near the entrance. In the vertical fracture model, CO_2 flow is very highly dispersed at the beginning, and no obvious dominant channel is formed.

The analysis shows that horizontal fractures serve as effective flow channels, enabling CO_2 to drive oil production quickly within the fractures; however, there is a high risk of gas channeling. Compared with horizontal fractures, vertical fractures facilitate better pore connectivity, and the CO_2 diffusion range is relatively uniform. In general, models with fractures have higher CO_2 sweep range and oil phase recovery factor in the same time than models without fractures.

3.4. *CO_2 storage mechanism*

In heterogeneous fractured reservoirs, CO_2 often flows along fractures in the early stage, bypassing significant volumes of the oil phase, and begins to diffuse laterally after the formation of high permeability channels (Seyyedi and Sohrabi, 2020). Fractures do not serve as CO_2 storage sites but can facilitate the transfer of CO_2 to pore throats. CO_2 is mainly stored in isolated pores away from the outlet, primarily through two mechanisms: capillary trapping of the free gas phase in the pore throat and dissolution in the oil and water phases.

As illustrated in Fig. 20(a), CO_2 enters isolated pores and displaces the oil phase. However, due to interfacial tension, capillary forces, and other factors, a portion of the CO_2 becomes trapped within these pores. When CO_2 displaces oil from a pore into a

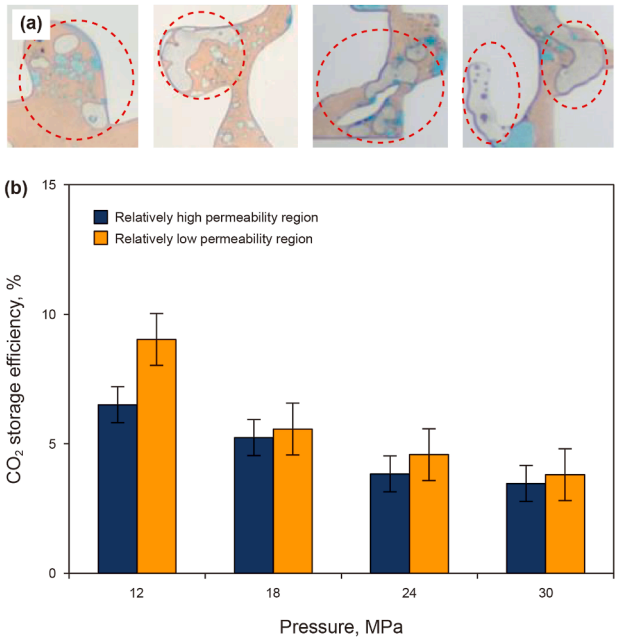

Fig. 20. Qualitative and quantitative characterization of CO_2 storage mechanism. (**a**) CO_2 storage site; (**b**) CO_2 storage efficiency.

narrow pore throat, the Jamin effect can further cause CO_2 to become trapped within the throat. It was also found that water has a significant impact on CO_2 storage. Under reservoir pressure, CO_2 will dissolve in water. Due to the hydrophilic nature of the pore walls, the water phase containing dissolved CO_2 adheres to the pore surfaces. This mechanism is particularly significant in water-wet reservoirs.

Furthermore, we quantitatively compared the CO_2 storage efficiency within the relatively high permeability and low permeability zones across varying pressure levels, as presented in Fig. 20(b). It is important to note that these statistics exclusively account for CO_2 sequestered within the oil and water phases. Free-phase CO_2 residing within pore spaces was deliberately excluded from the calculation. This exclusion stems from the high probability of such CO_2 migrating out through pore throats, a phenomenon governed by breakthrough pressure thresholds, which, if included, would likely introduce significant error into the storage efficiency quantification. The results indicate that the larger residual oil and water saturation area within the relatively low permeability zone correlates with a higher volume of internally stored CO_2, consequently yielding a greater CO_2 storage efficiency percentage for this zone. Conversely, increasing pressure facilitates the displacement of oil and water from the pores, leading to a corresponding decline in the CO_2 storage percentage. Minor uncertainties are inherent in the calculations due to the reliance on CO_2 solubility data in oil; however, these potential errors remain within acceptable margins.

Due to the presence of heterogeneity, CO_2 migrating into the low permeability region is more likely to be stored. As shown in Fig. 14, the pores in which the residual oil is still unable to be produced under increasing pressure seem to be good gas storage sites. In general, CO_2 huff-n-huff can not only improve recovery factor, but also contribute to CO_2 storage.

4. Conclusions

In this paper, the microscopic displacement mechanism, residual oil distribution, and CO_2 storage characteristics in heterogeneous fractured reservoirs were investigated through physical experiments and numerical simulation. The following conclusions can be drawn:

(1) At an injection pressure of 12 MPa, compared with continuous displacement, the huff-n-huff process can more effectively mobilize the oil phase in low permeability regions and mitigate the influence of heterogeneity. Supercritical CO_2 huff-n-huff achieves a recovery factor of 13.25% higher than that of water huff-n-huff, indicating the best production performance of CO_2 huff-n-huff among the tested methods.
(2) Under water-wet conditions, the water phase is either adsorbed onto the pore walls or surrounds the oil phase, creating resistance to oil flow. Residual oil mainly forms because the driving force during huff-n-puff is insufficient to overcome this resistance. The residual oil primarily exhibits porous and columnar morphologies, distributed nearly equally between the relatively low permeability and high permeability regions (ratio close to 1:1). With prolonged soaking time, the proportions of cluster, film-liked, and porous residual oil decrease, while the proportion of columnar residual oil increases, and proportion of isolated-pore residual oil remains unchanged. When the soaking time and injection pressure increase to a certain extent, further increases have diminishing effects on CO_2 displacement efficiency.
(3) The diffusion coefficient of CO_2 in the oil phase ranges from 7.48×10^{-9} to 19.5×10^{-9} m^2/s. When the pressure exceeds the minimum miscibility pressure (MMP) of CO_2, the diffusion coefficient increases significantly, leading to a notably expanded swept area in isolated pores and pore throats distant from fractures and the outlet. When the diffusion coefficient is increased by 10 times, the diffusion range of CO_2 increases significantly at the same time.
(4) In the absence of fractures, high permeability channels are easily formed during CO_2 displacement. Horizontal fractures provide effective pathways for fluid migration, while vertical fractures exhibit strong pore-connectivity capacity, both of which can effectively enhance the diffusion range of CO_2.
(5) A portion of CO_2 is stored as bubbles in isolated pores surrounded by water and oil phases, while another portion remains dissolved in the oil phase and retained as part of the residual oil–gas mixture. A higher CO_2 storage efficiency in both the oil and water phases is observed in regions with relatively low permeability, compared to those with higher permeability.

CRediT authorship contribution statement

Nan Chen: Writing – original draft, Investigation, Formal analysis, Data curation, Conceptualization. **Chuan-Jin Yao:** Writing – review & editing, Validation, Supervision, Funding acquisition. **Bai-Shuo Liu:** Writing – review & editing, Supervision. **Jia Zhao:** Supervision. **Cui-Fang Li:** Supervision.

Declaration of competing interest

The authors declare that they have no known competing financial interests or personal relationships that could have appeared to influence the work reported in this paper.

Acknowledgments

This work is financially supported by the National Natural Science Foundation of China (Nos. 52574075, U22B6004) and the Shandong Provincial Natural Science Foundation (No. ZR2024ME083). We also appreciate the reviewers and editors for their constructive comments to make the paper high quality.

Appendix A

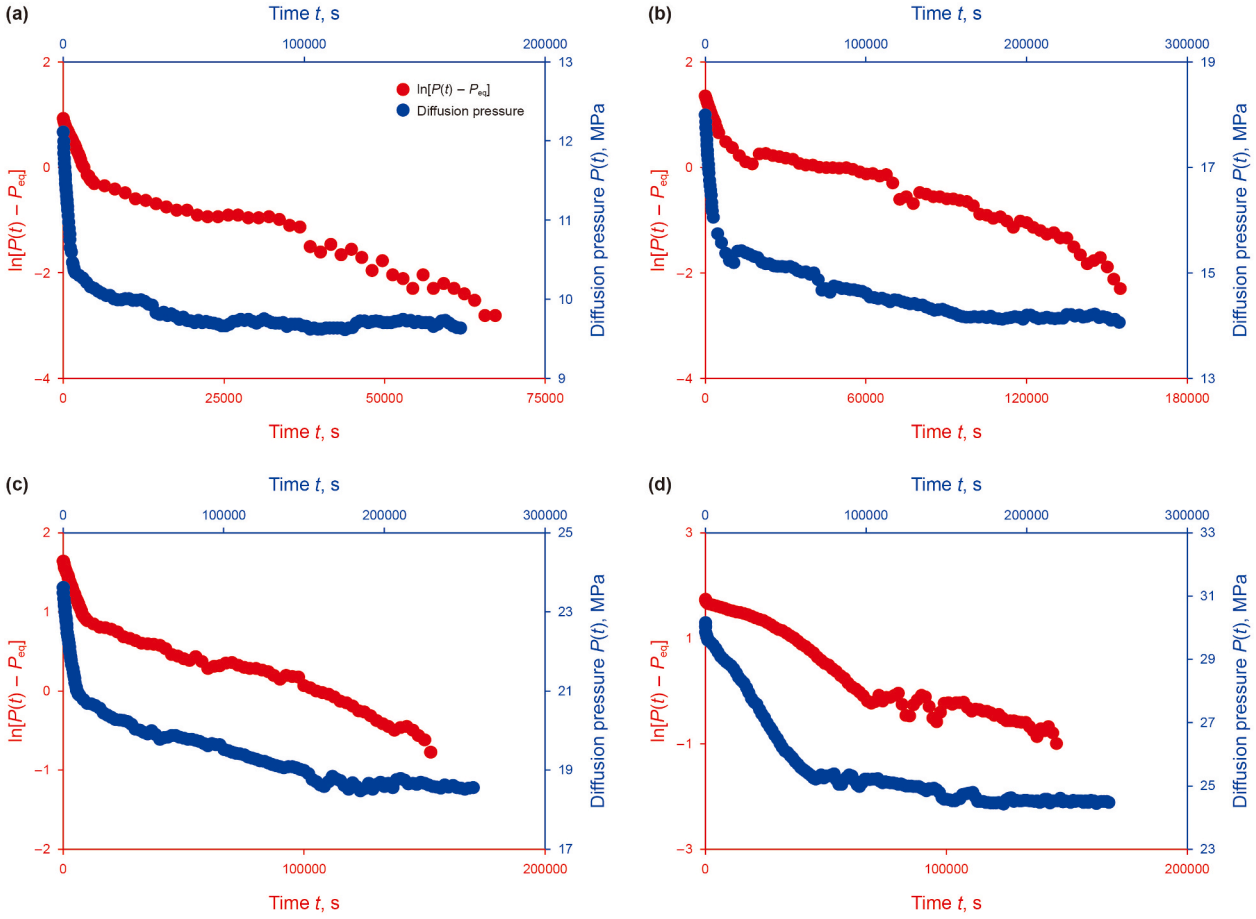

Fig. A1. Variation of CO_2–oil diffusion pressure at different pressures: (**a**) 12 MPa, (**b**) 18 MPa, (**c**) 24 MPa, (**d**) 30 MPa.

References

Abedini, A., Mosavat, N., Torabi, F., 2014. Determination of minimum miscibility pressure of crude oil–CO_2 system by oil swelling/extraction test. Energy Technol. 2 (5), 431–439. https://doi.org/10.1002/ente.201400005.

Alfarge, D., Wei, M., Bai, B.,., et al., 2017. Effect of molecular-diffusion mechanisim on CO_2 huff-n-puff process in shale-oil reservoirs. In: SPE Kingdom of Saudi Arabia Annual Technical Symposium and Exhibition. https://doi.org/10.2118/188003-MS.

Al-Khdheeawi, E., Vialle, S., Barifcani, A., et al., 2017. Impact of reservoir wettability and heterogeneity on CO_2-plume migration and trapping capacity. Int. J. Greenh. Gas Control 58, 142–158. https://doi.org/10.1016/j.ijggc.2017.01.012.

Al-Khdheeawi, E., Vialle, S., Barifcani, A., et al., 2018. Effect of wettability heterogeneity and reservoir temperature on CO_2 storage efficiency in deep saline aquifers. Int. J. Greenh. Gas Control 68, 216–229. https://doi.org/10.1016/j.ijggc.2017.11.016.

British Petroleum, 2020. Statistical Review of World Energy 2020, 69th edition https://www.bp.com/content/dam/bp/business-sites/en/global/corporate/pdfs/energy-economics/statistical-review/bp-stats-review-2020-full-report.pdf.

Chang, C., Zhou, Q., Kneafsey, T., et al., 2016. Pore-scale supercritical CO_2 dissolution and mass transfer under imbibition conditions. Adv. Water Resour. 92, 142–158. https://doi.org/10.1016/j.advwatres.2016.03.015.

Chen, Z., Li, R., Yang, S., et al., 2024. A novel algorithm for asphaltene precipitation modeling in shale reservoirs with the consideration of capillary pressure during the CCUS processes. Appl. Therm. Eng. 248, 123217. https://doi.org/10.1016/j.applthermaleng.2024.123217.

Ding, J., Yan, C., He, Y., et al., 2021. Supercritical CO_2 sequestration and enhanced gas recovery in tight gas reservoirs: Feasibility and factors that influence efficiency. Int. J. Greenh. Gas Control 105, 103234. https://doi.org/10.1016/j.ijggc.2020.103234.

Doughty, C., Pruess, K., 2004. Modeling supercritical carbon dioxide injection in heterogeneous porous media. Vadose Zone J. 3 (3), 837–847. https://doi.org/10.2136/vzj2004.0837.

Fang, Y., Yang, E., Guo, S., et al., 2022. Study on micro residual oil distribution of polymer flooding in Class-II B oil layer of Daqing Oilfield. Energy 254, 124479. https://doi.org/10.1016/j.energy.2022.124479.

Ghasemi, M., Astutik, W., Alavian, S., 2017. Determining diffusion coefficients for carbon dioxide injection in oil-saturated chalk by use of a constant-volume-diffusion method. SPE J. 22 (2), 505–520. https://doi.org/10.2118/179550-PA.

Greig, C., Uden, S., 2021. The value of CCUS in transitions to net-zero emissions. Electr. J. 34 (7), 107004. https://doi.org/10.1016/j.tej.2021.107004.

Guo, Y., Liu, F., Qiu, J., et al., 2022. Microscopic transport and phase behaviors of CO_2 injection in heterogeneous formations using microfluidics. Energy 256, 124524. https://doi.org/10.1016/j.energy.2022.124524.

Huang, F., Xu, R., Jiang, P., et al., 2020. Pore-scale investigation of CO_2/oil exsolution in CO_2 huff-n-puff for enhanced oil recovery. Phys. Fluids 32 (9). https://doi.org/10.1063/5.0021107.

Huang, X., Gu, L., Li, S., 2022. Absolute adsorption of light hydrocarbons on organic-rich shale: An efficient determination method. Fuel 308, 121998. https://doi.org/10.1016/j.fuel.2021.121998.

Jayne, R., Wu, H., Pollyea, R., 2019. Geologic CO_2 sequestration and permeability uncertainty in a highly heterogeneous reservoir. Int. J. Greenh. Gas Control 83, 128–139. https://doi.org/10.1016/j.ijggc.2019.02.001.

Jia, P., Guo, H., Wang, Y., et al., 2022. COMSOL-based investigation of the characteristics of microscopic water flooding and residual oil distribution in carbonate reservoirs. Front. Earth Sci. 10, 1016941. https://doi.org/10.3389/feart.2022.1016941.

Lei, Z., Liu, Y., Wang, R., 2022. A microfluidic experiment on CO_2 injection for enhanced oil recovery in a shale oil reservoir with high temperature and pressure. Energies 15 (24), 9461. https://doi.org/10.3390/en15249461.

Li, D., Saraji, S., Jiao, Z., et al., 2021. CO_2 injection strategies for enhanced oil recovery and geological sequestration in a tight reservoir: An experimental study. Fuel 284, 119013. https://doi.org/10.1016/j.fuel.2020.119013.
Li, L., Sheng, J., Su, Y., et al., 2018. Further investigation of effects of injection pressure and imbibition water on CO_2 huff-n-puff performance in liquid-rich shale reservoirs. Energy Fuels 32 (5), 5789–5798. https://doi.org/10.1021/acs.energyfuels.8b00536.
Liang, B., Chen, C., Jia, C., et al., 2024. Carbon capture, utilization and storage (CCUS) in oil and gas reservoirs in China: Status, opportunities and challenges. Fuel 375, 132353. https://doi.org/10.1016/j.fuel.2024.132353.
Liu, X., Jia, X., Niu, Y., et al., 2023. Alterations in coal mechanical properties and permeability influenced by liquid CO_2 phase change fracturing. Fuel 354, 129254. https://doi.org/10.1016/j.fuel.2023.129254.
Liu, Y., Lv, P., Liu, Y., et al., 2016. CO_2/water two-phase flow in a two-dimensional micromodel of heterogeneous pores and throats. RSC Adv. 6 (77), 73897–73905. https://doi.org/10.1039/C6RA10229H.
Luo, J., Hou, Z., Feng, G., 2022. Effect of reservoir heterogeneity on CO_2 flooding in tight oil reservoirs. Energies 15 (9), 3015. https://doi.org/10.3390/en15093015.
Lv, Q., Zheng, R., Zhou, T., et al., 2022. Visualization study of CO_2-EOR in carbonate reservoirs using 2.5 D heterogeneous micromodels for CCUS. Fuel 330, 125533. https://doi.org/10.1016/j.fuel.2022.125533.
Nguyen, P., Carey, J., Viswanathan, H., et al., 2018. Effectiveness of supercritical-CO_2 and N_2 huff-and-puff methods of enhanced oil recovery in shale fracture networks using microfluidic experiments. Appl. Energy 230, 160–174. https://doi.org/10.1016/j.apenergy.2018.08.098.
Qiu, J., Tang, W., Bao, B., et al., 2021. Microfluidic-based in-situ determination for reaction kinetics of hydrogen peroxide decomposition. Chem. Eng. J. 424, 130486. https://doi.org/10.1016/j.cej.2021.130486.
Rossen, W., 2017. Foams in enhanced oil recovery. In: Prud'Homme, R.K., Khan, S.A. (Eds.), Foams, pp. 413–464.
Seyyedi, M., Sohrabi, M., 2020. Oil reservoir on a chip: Pore-scale study of multiphase flow during near-miscible CO_2 EOR and storage. Transport Porous Media 134 (2), 331–349. https://doi.org/10.1007/s11242-020-01448-3.
Sheng, J., 2017. Critical review of field EOR projects in shale and tight reservoirs. J. Pet. Sci. Eng. 59, 654–665. https://doi.org/10.1016/j.petrol.2017.09.022.
Smirnova, E., Kot, S., Kolpak, E., et al., 2021. Governmental support and renewable energy production: A cross-country review. Energy 230, 120903. https://doi.org/10.1016/j.energy.2021.120903.
Song, C., Yang, D., 2017. Experimental and numerical evaluation of CO_2 huff-n-puff processes in Bakken Formation. Fuel 190, 145–162. https://doi.org/10.1016/j.fuel.2016.11.041.
Sun, L., Bai, B., Wei, B., et al., 2019. Recent advances of surfactant-stabilized N_2/CO_2 foams in enhanced oil recovery. Fuel 241, 83–93. https://doi.org/10.1016/j.fuel.2018.12.016.
Tang, W., Sheng, J., 2022. Huff-n-puff gas injection or gas flooding in tight oil reservoirs? J. Pet. Sci. Eng. 208, 109725. https://doi.org/10.1016/j.petrol.2021.109725.
Wei, B., Zhang, X., Wu, R., et al., 2019. Pore-scale monitoring of CO_2 and N_2 flooding processes in a tight formation under reservoir conditions using nuclear magnetic resonance (NMR): A case study. Fuel 246, 34–41. https://doi.org/10.1016/j.fuel.2019.02.103.
Wu, X., Tian, Z., Guo, J., 2022. A review of the theoretical research and practical progress of carbon neutrality. Sustain. Oper. Comput. 3, 54–66. https://doi.org/10.1016/j.susoc.2021.10.001.
Zhang, K., Jia, N., Liu, L., 2019a. CO_2 storage in fractured nanopores underground: Phase behaviour study. Appl. Energy 238, 911–928. https://doi.org/10.1016/j.apenergy.2019.01.088.
Zhang, K., Jia, N., Li, S., et al., 2019b. Static and dynamic behavior of CO_2 enhanced oil recovery in shale reservoirs: Experimental nanofluidics and theoretical models with dual-scale nanopores. Appl. Energy 255, 113752. https://doi.org/10.1016/j.apenergy.2019.113752.
Zhang, M., Li, B., Lei, W., et al., 2024. Oil displacement and CO_2 storage during CO_2 immiscible huff-n-puff within a saturated reservoir: An experimental study. Fuel 371, 2026. https://doi.org/10.1016/j.fuel.2024.132026.
Zhang, X., Li, L., Su, Y., et al., 2023. Microfluidic investigation on asphaltene interfaces attempts to carbon sequestration and leakage: Oil-CO_2 phase interaction characteristics at ultrahigh temperature and pressure. Appl. Energy 348, 121518. https://doi.org/10.1016/j.apenergy.2023.121518.
Zhang, Y., Hyndman, C., Maini, B., 2000. Measurement of gas diffusivity in heavy oils. J. Pet. Sci. Eng. 25 (1–2), 37–47. https://doi.org/10.1016/S0920-4105(99)00031-5.
Zhao, Y., Zhang, Y., Lei, X., et al., 2020. CO_2 flooding enhanced oil recovery evaluated using magnetic resonance imaging technique. Energy 203, 117878. https://doi.org/10.1016/j.energy.2020.117878.
Zhong, H., He, Y., Yang, E., et al., 2022. Modeling of microflow during viscoelastic polymer flooding in heterogenous reservoirs of Daqing Oilfield. J. Pet. Sci. Eng. 210, 110091. https://doi.org/10.1016/j.petrol.2021.110091.
Zuloaga, P., Yu, W., Miao, J., et al., 2017. Performance evaluation of CO_2 huff-n-puff and continuous CO_2 injection in tight oil reservoirs. Energy 134, 181–192. https://doi.org/10.1016/j.energy.2017.06.028.